THE ASTROPHYSICAL JOURNAL, 435:261–273, 1994 November 1

MULTIPLE OUTFLOW EPISODES FROM PROTOSTARS: THREE-DIMENSIONAL MODELS OF INTERMITTENT JETS

ELISABETE M. DE GOUVEIA DAL PINO
University of São Paulo, Instituto Astronômico e Geofisico, Av. Miguel Stéfano, 4200, São Paulo, SP 04301-904, Brazil.
E-Mail: dalpino@astro1.iagusp.usp.br

AND

WILLY BENZ
University of Arizona, Steward Observatory, and Lunar and Planetary Laboratory, Tucson, AZ 85721
Received 1994 January 24; accepted 1994 May 3

ABSTRACT

We present fully three-dimensional simulations of supersonic, radiatively cooling intermittent jets with intermediate and long variability periods (that is, periods of the order of, or longer than, the dynamical timescale of the jet, $\tau \geq \tau_{dy}$, where $\tau_{dy} \equiv R_j/v_j$. Variations of intermediate period elucidate the formation and evolution of chains of internal regularly spaced radiative shocks, which in this work are identified with the observed emission knots of protostellar jets. Variations of long period elucidate the formation of multiple bow shock structures separated by long trails of diffuse gas, which resemble those observed in systems like HH 111 and HH 46/47. The time variability of the outflow is probably associated with observed irruptive events in the accretion process around the protostars. In our simulations, the outflow variations are produced by periodically *turning on* the outflow with a highly supersonic velocity and periodically *turning off* it to a low-velocity regime. When a supersonic parcel finds the flow material that has been injected earlier, a double shock structure promptly develops: a *forward* shock sweeps up the slow material ahead of it and a *reverse* shock decelerates the fast material behind. The very high density contrast between the fast and slow portions of the flow causes the *reverse* shock to be much weaker than the *forward* shock so that line emission by gas between these shocks is essentially single peaked.

In the case of velocity variations of *intermediate* period, we find, as in previous work, that the shock structures form a train of regularly spaced emitting features which move away from the source with a velocity close to that of the outflow, have high radial motions, and produce low-intensity spectra, as required by the observations. As they propagate downstream, the shocks widen and dissipate due to the expulsion of material sideways to the cocoon by the high pressure gradients of the postshock gas. This fading explains the most frequent occurrence of knots closer to the driving source. The head structure of these outflows is very affected by interactions with the internal knots.

In the case of the *long*-period velocity variability, our simulations have produced a pair of bowshock–like structures separated by a trail almost starved of gas extending for many jet radii in agreement with the observations. The leading bow shock or working surface developed at the head of the jet has a similar structure to that of steady jets (e.g., Gouveia Dal Pino & Benz 1993): the dense shell formed from the condensation of the shock-heated gas also fragments into a clumpy structure and becomes thermally unstable. Parts of the shell spill into the cocoon forming an extended narrow plug. The narrowing of the jet head causes some beam acceleration. The bow shock produced from the second injection propagates downsteam on the diffuse tail behind the leading working surface. It has a double shock structure similar to the one of the leading working surface and on average propagates faster. The postshock radiative material also cools and forms a cold shell whose density is much smaller than that of the shell of the leading working surface. This result is consistent with observations that suggest that the emission of the internal working surface is of lower intensity and excitation than that of the leading working surface.

A brief discussion on the possibility of these time-dependent intermittent jets to drive molecular outflows is also presented.

Subject headings: hydrodynamics — ISM: individual (HH 46/47, HH 111) — ISM: jets and outflows — shock waves — stars: pre–main-sequence

1. INTRODUCTION

Most protostellar jets show a bow shock–like structure at the edge of the beam which is identified as the jet working surface (for reviews see, for example, Mundt 1988; Reipurth 1989a). As the supersonic jet propagates into the ambient gas, it develops a shock pattern at the head. A detailed three-dimensional numerical analysis of this shock pattern for continuous flows has been done in a previous paper (Gouveia Dal Pino & Benz 1993a, hereafter Paper I). The beam outflow is decelerated in a jet shock or Mach disk, whereas the impacted ambient material is accelerated by the forward bow shock. In some jets (e.g., HH 46/47 and HH 111), there is clear evidence of two or more such bow shock structures separated by a trail of diffuse gas for many jet radii (e.g., Hartigan, Raymond, & Meaburn 1990; Reipurth 1989b). These multiple bow shocks have been interpreted as evidence for distinct outflow episodes

from the jet source (e.g., Reipurth 1989b; Raga et al. 1990; Reipurth & Heathcote 1991; Gouveia Dal Pino & Benz 1993b, c).

Usually, along the jet beam, there is a chain of rather regularly spaced emission knots with large proper motions (~ 50–300 km s^{-1}), emitting mainly low-excitation lines. The knots often become fainter and disappear at larger distances from the source, as for example, in the HH 34 and HH 111 jet systems (e.g., Reipurth et al. 1986; Reipurth 1989b; Morse et al. 1992; Reipurth, Raga, & Heathcote 1992). It is generally believed that the line emission is produced by shock-heated gas in the jet flow (e.g., Hartigan, Raymond, & Hartmann 1987).

The precise nature of the mechanism that produces these internal shocks is still controversial. One of the possibilities is that the shocks are driven by Kelvin-Helmholtz (K–H) instabilities excited in the interface between the jet flow and the surrounding medium (e.g., Birkinshaw 1991). This mechanism has been examined in detail in two-dimensional (Blondin, Fryxell, & Königl 1990, hereafter BFK) and three-dimensional (Paper I) hydrodynamic simulations of steady state radiative cooling jets which showed that, under the presence of radiative cooling, shocks driven by K-H instabilities are fainter and less numerous than in adiabatic jets. The radiative cooling reduces the thermal pressure which is deposited in the cocoon that surrounds the beam. As a result, the cocoon has less pressure to collimate, drive K-H instabilities, and, thus, reflect internal shocks in the beam. Although this mechanism remains viable, it probably plays a secondary role in the production of internal shocks.

A more attractive possibility is that the knots (like the multiple bow shocks) could be the product of time variations in the ejection mechanism that produces the jet. Strong support for this argument comes from recent high resolution observations of the HH 34 and HH 111 jets (Morse et al. 1993) which, based on the morphology, spectra, and kinematics of the knots, show evidence of a velocity-variable outflow with multiple ejections. Also, long-slit spectra of HH 83 and HH 46/47 show that the radial velocity of the emitting material increases with increasing distance from the source. In the case of HH 46/47, abrupt variations of this velocity have been detected (e.g., Reipurth 1989a, b). These data are consistent with variable jet ejection velocity where the knots would be the products of multiple outflow episodes.

The time variability of the outflow is probably associated with irruptive events in the accretion process around the protostar (e.g., Dopita 1978; Reipurth 1985). In fact, some energy sources of protostellar jets and HH objects, as for example the sources of HH 57 and HH 28/29 (e.g., Reipurth 1989b), have been seen to erupt into FU Orionis outbursts. These episodes could produce massive ejections along the stellar jets every 100–1000 yr (e.g., Hartigan & Raymond 1992; Hartmann, Kenyon, & Hartigan 1993), suggesting that the driving sources can change on timescales shorter than the dynamical timescale of the HH objects.

The possibility that internal knots could emerge from variations in the ejection mechanism was first proposed by Rees (1978) in the context of extragalactic jets. He showed that time variations of the supersonic ejection velocity would produce internal shocks that would travel along the beam. Later, Wilson (1984) performed two-dimensional numerical simulations of pulsating adiabatic jets and showed that the internal shocks evolve to two-shock *internal working surface* structures. More recently, Raga et al. (1990) developed a one-dimensional analytical model employing the Burgers equation of motion, which neglects the gas pressure gradient forces in the beam to describe the evolution of high Mach number flows from time-dependent sources. Their results qualitatively confirmed the predictions of previous work. Pursuing this idea further, Kofman & Raga (1992, hereafter KR), assuming a constant jet density, and Raga & Kofman (1992, hereafter, RK), assuming a constant jet density, extended that study and derived analytic asymptotic solutions of the Burgers equation for the jet flow at large distances from the source. They found that the flow would consist of continuous segments for which the flow velocity would increase linearly with the distance from the source, separated by discontinuous velocity jumps which should correspond to the knots or internal working surfaces propagating down the flow at the mean flow velocity. Using similar assumptions, Raga (1992) studied the evolution of random perturbations in the jet velocity. Although their results partially reproduce the observations, they cannot correctly describe the time evolution of the density and velocity profiles of the knots as the pressure has been neglected. In such cases, the motion of the knots is essentially determined from simple ram pressure balance. This assumption is valid only in the region close to the jet axis or if the flow is surrounded by a high density gas at rest. A generalization of their work by Hartigan & Raymond (1992, hereafter HIR) took into account the pressure effects, performed one-dimensional numerical hydrodynamical calculations of pulsating cooling jets, and evaluated the evolution and intensity of the pulses along the jet axis. To compute the radiative losses of the flow they used a detailed time-dependent nonequilibrium model.

Although all those calculations qualitatively (and quantitatively) reproduce some of the observational properties of the protostellar knots (e.g., proper motions, emission-line intensities, knot spacing), they all have assumed one-dimensional flows. In general, sudden changes of the jet radius and the velocity are expected at the position of the internal knots. This results in a shock structure which is more complex than the one described by the one-dimensional approach and in which the effects of the thermal pressure are nonnegligible. A multidimensional analysis is then required for a self-consistent calculation of the structure and dynamics of these jets from time dependent sources. Very recently, Falle & Raga (1993) performed two-dimensional numerical calculations of individual internal working surfaces. In this work, we present fully three-dimensional numerical simulations of supersonic radiative jets with variable ejection velocity, in order to examine the formation and evolution of chains of internal knots and also the formation of the multiple bow shocks which are observed to be separated by large portions of very diffuse and almost invisible flow. Fully three-dimensional simulations can provide a complete description of the flow kinematics at any time in the evolution, subject to the constraints of numerical resolution.

In order to represent the velocity variability, we assume that the jet is periodically "turned on" with a full supersonic velocity and periodically "turned off" to a small velocity. In such "intermittent" jets, the velocity perturbations are of large amplitude and are accompanied by similar density enhancements (see also HR). To study the development of a chain of internal knots along the jet, we consider velocity variations with a period comparable to the dynamical time scale of the jet (which we define in this work as being $\tau_{dy} \equiv R_j/v_j$, where R_j is the jet radius and v_j is the mean jet velocity). To investigate the

formation of multiple bow shock structures separated by long trails of diffuse gas, on the other hand, we assume variations with much longer periods than the jet dynamical time scale.

In Paper I, we presented the first fully three-dimensional simulations of radiative cooling jets ejected at a constant velocity using the smoothed particle hydrodynamics technique (SPH). In a subsequent paper (Chernin et al. 1994, hereafter Paper II), we employed the same technique to study the dynamics of the transfer of momentum from jets to ambient molecular clouds in order to examine the correlation between protostellar jets and molecular outflows. In the present work, we use a modified version of the code employed in these previous investigations. Contemporaneously with this work, Stone & Norman (1993a, hereafter SN) have performed two- and three-dimensional simulations of pulsed cooling jets in which the jet velocity is assumed to undergo sinusoidal small amplitude ($\Delta v/v_j \ll 1$, where Δv is the maximum velocity variation) high-frequency oscillations ($\tau < t_j = R_j/c_a$, where c_a is the sound speed of the ambient medium). In their simulations, the density is pulsed inversely with the velocity in order to keep the mass flux constant. Although in our simulations we have assumed higher amplitude, smaller frequency velocity and density variations ($\Delta v/v_j \simeq 1$, $\tau \geq t_j > \tau_{dy}$), where both investigations overlap, the results are qualitatively similar.

The organization of this work is as follows. In § 2, we discuss briefly the basic theoretical properties of intermittent jets and describe the assumptions of our numerical model, including the initial and boundary conditions, and model parameters adopted for the simulations. In § 3, we present the results of our hydrodynamical simulations for jets with both intermediate and long-period velocity variations of high amplitude. Finally, in § 4, we summarize our results and discuss their possible applications to the observed protostellar jets.

2. DESCRIPTION OF THE MODEL

2.1. *Theoretical Grounds*

The basic properties of jets with continuous injection are described in Paper I. Jets with supersonic variations in the velocity are expected to produce shock waves along the outflow as the fast material overtakes the slower material (e.g., Raga et al. 1990; HR). In general, a pair of shocks must form as the supersonic velocity perturbation steepens. A downstream (or forward) shock is produced as the perturbation sweeps up the low-velocity material ahead of it and an upstream (or reverse) shock must decelerate the fast material that collides with the perturbation. This shock structure resembles the working surface that appears at the head of the jet where the forward shock is identified with the bow shock and the reverse shock with the jet shock (e.g., BFK; Paper I).

As we have mentioned earlier, the protostellar jets display a large number of emitting knots, which in the present work we identify with internal *working surfaces*. So, in order to reproduce such a structure, one would require

$$N_{is} \approx \frac{f\tau_{dy}}{\tau} \gg 1 \tag{1}$$

internal working surfaces, where τ_{dy} is the dynamical timescale of the flow $\tau_{dy} \equiv R_j/v_j$; $f = L/R_j$, L being the total length of the outflow; and τ the period of the velocity variability. Condition (1) could be used, in principle, to predict the variability period required for producing a given number of internal knots observed in an outflow.

One-dimensional analysis can give an estimate of the velocity of propagation of an internal working surface. This velocity can be evaluated by balancing the momentum flux of the flow upstream with the momentum flux of the flow downsteam of the working surface. If the velocity upsteam of the working surface is v_u and the velocity downsteam is v_d, then the propagation velocity of the internal working surface, v_{is}, is given by

$$\rho_u(v_u - v_{is})^2 + p_u \simeq \rho_d(v_{is} - v_d)^2 + p_d\,, \tag{2}$$

where ρ_u and ρ_d are the mass densities up and downstream, and p_u and p_d are the thermal pressures up and downstream, respectively. For highly supersonic flows or under the condition of thermal pressure balance, $p_u - p_d$ can be neglected and the internal working surface velocity is then roughly given by

$$v_{is} \simeq \frac{\beta v_u + v_d}{1 + \beta}\,, \tag{3}$$

where $\beta = (\rho_u/\rho_d)^{1/2}$. We see that for $\beta = (\rho_u/\rho_d)^{1/2} \gg 1$

$$v_{is} \simeq (1 - \beta^{-1})v_u\,, \tag{4}$$

We note that equations (3) and (4) must be satisfied only in the region close to the axis of symmetry of the jet, as pressure gradient effects must be nonnegligible off the axis (see below).

The primary aim of the present work is to study the dynamical evolution of jets with high-amplitude velocity discontinuities of intermediate and long period which must steepen to form shocks. A jet that varies in velocity is likely to vary in density as well. As has been argued by HR, without an understanding of the mechanism that generates the stellar jets, it is not clear whether the density varies with the velocity or inversely with the velocity keeping the mass flux constant (as has been assumed by SN). In the simulations of "intermittent" jets presented here, both the fast flow portions (ejected in the "turning on" phases) and the slow portions (ejected during the "quiescent" phases) are ejected with the same initial density. However, during the quiescent phase, a trail of very diffuse gas develops behind the previous fast portion of flow. As a consequence, when a new fast flow portion emerges from the inlet, it finds a downstream slow flow portion of low density. A similar scenario has also been investigated in some of the one-dimensional models of HR and they found that in such cases, the forward (downstream) shock is much stronger than the reverse (upstream) shock. (This situation resembles the bullet models of Norman & Silk 1979, as we are going to see below.) In the case that the mass-loss flux is kept constant, the high-velocity flow will be less dense than the low-velocity one, and in this case, the reverse shock is expected to have larger velocity than the forward shock (see HR and SN).

2.2. *The Numerical Model*

We solve the hydrodynamics conservation equations using the smoothed particle hydrodynamics technique (SPH). As in Paper I, we use a version of the three-dimensional Cartesian SPH code (described in detail by Benz 1990, 1991) modified to include the effects of cooling. SPH is a Lagrangean approach to fluid dynamics which does not require the use of a fixed grid for the computation of the derivatives but instead employs particles which track the fluid and move with it. Each SPH particle is characterized by its position in the six-dimensional phase-space ($\boldsymbol{r}$, $\boldsymbol{v}$), its mass, and its specific internal energy. The SPH particles are smoothed out in space by a spherically symmetric kernel function of width h. The initial values of h were,

in general, chosen to be 0.4 and $0.2R_j$, for the ambient and the jet particles, respectively.

As in Paper I, the jet and the ambient gas are treated as a single, fully ionized fluid with a ratio of specific heats $\gamma = 5/3$ and an ideal equation of state $p = u(\gamma - 1)\rho$, where u is the internal energy per unit mass, p is the thermal pressure, and $\rho = n\bar{m}$ is the mass density, where n is the particle number density and $\bar{m}$ is the mean mass per particle which remains constant in the case of complete ionization.

Radiative cooling (due to collisional excitation and deexcitation, and recombination) is implicitly calculated using the *local* time-independent cooling function evaluated by Katz (1989) for a gas of cosmic abundances cooling from $T = 10^6$ K. The cooling is suppressed below $T \approx 8000$ K when the assumption of completely ionized flow breaks down and the effects of transfer of ionizing radiation become important. For $T < 8000$ K, the radiative cooling is mainly due to the formation of molecules and molecular lines, and, therefore, the expected overall cooling will be stronger than that inferred in our calculations. By not taking into account the effects of nonequilibrium ionization of the gas or the transfer of ionizing radiation, we are probably underestimating the cooling rate in some parts of the postshock regions by as much as an order of magnitude (e.g., Innes, Giddings, & Falle 1987). However, a comparison of our results (see also Paper I) with the calculations of SN (and also with recent multidimensional calculations for steady flows; Stone & Norman 1993b), which have included a nonequilibrium time-dependent cooling, show that the essential dynamical features do not change under the presence of nonequilibrium ionization effects.

As pointed out in Paper I and II, in SPH simulations the properties of the low-density regions, as for example, the cocoon that develops between the swept-up ambient gas and the jet beam, or the region between successive knots along the beam (see below) are poorly sampled because they do not contain as many SPH particles as the denser regions. However, one of the advantages of SPH codes over grid-based codes is not having to calculate properties of "empty" regions. These low-density regions may become a problem only if their pressure is dynamically significant, but we later show that this is not the case. Another limitation of SPH simulations is its treatment of turbulence, which is expected to be significant in protostellar jets since the inferred Reynolds numbers are of the order $Re \simeq 10^4$–10^5. This difficulty is mainly due to the fact that the numerical viscosity in the code (see Paper I) may be too dissipative and the particle size is orders of magnitude larger than the Kolmogorov dissipation scale, $\sim d_{\rm cool}/Re < R_j/10^4$. However, the main effect of this viscosity is to suppress numerical instabilities which develop on scales smaller than the scale fixed by the viscosity law. If the number of SPH particles is increased, thereby increasing the resolution of the simulations, smaller scale eddies are seen, but the large-scale structures of the flow remain the same. Thus, our simulations are adequate for studying the gross properties of the jet system.

The boundary conditions are the same as described in Paper I. All distances are normalized to the jet radius R_j. An initially homogeneous ambient gas fills the spatial domain which has dimensions of 24 or $45R_j$ in the z-axis direction and $-6R_j \leq x$, $y \leq 6R_j$ in the transverse directions. A jet with a circular cross section is injected at $z = 0$ in the middle of the "ambient box" and allowed to propagate. We assume periodic boundary conditions on the x and y peripheries (see Paper I) and continuitive boundary conditions at $z = 0$ and $z_{\rm max}$. (These conditions are different from those in the three-dimensional simulations of SN who assumed reflecting boundaries on the midplanes $x = 0$, $y = 0$ of the jet. In such cases the jet is symmetric across both planes. This assumption prohibits the development of nonaxisymmetric modes of dynamical instabilities in the beam.)

The evolution of the system is characterized by the dimensionless parameters: (i) $\eta = \rho_j/\rho_a$ (the ratio beteen the input jet and ambient densities); (ii) $M_a = v_j/c_a$ [the initial ambient Mach number, where the ambient sound speed is given by $c_a = (\gamma kT_a/\bar{m})^{1/2}$, with T_a being the initial ambient temperature and $\bar{m} \simeq 0.5m_{\rm H}$ the mean mass per particle for a fully ionized gas of cosmic abundances]; (iii) $k_p = p_j/p_a$ (the input pressure ratio which has been assumed to be initially equal to unity in all simulations); and (iv) $q_{\rm bs}$ [the ratio of the cooling length in the postshock gas behind the bow shock (at the jet head) to the jet radius (see eq. [7] of Paper I), which, for shock velocities $v_s > 90$ km s^{-1} is related to the ratio measured in the postshock gas behind the jet shock $q_{\rm js}$ through $q_{\rm js} \simeq q_{\rm bs}\eta^{-3}$ (see eq. [8] of Paper I)].

The parameters of the simulations were chosen to resemble the conditions found in protostellar jets. The densities of protostellar jets are not well determined. Early estimates indicated jet number densities $n_j \equiv \eta n_a \sim 20$–$100$ cm^{-3} (e.g., Mundt, Brügel, & Bührke 1987, hereafter MBB), but recent observations seem to indicate values larger than 10^3 cm^{-3} (e.g., Morse et al. 1992, 1993). The density ratio η is even more uncertain. Observations suggest values $\eta \simeq 1$–20 (e.g., MBB; Morse et al. 1992; Raga & Noriega-Crespo 1993). Typical jet velocities have been determined from proper motions and radial velocities of the knots and range from $v_j \simeq 100$–500 km s^{-1} (e.g., Reipurth 1989b; Reipurth et al. 1992), corrsponding to jet temperatures $T_j = \eta^{-1}T_a \simeq 10^4$ K. Typical jet radii are 0.5–4×10^{16} cm (e.g., MBB). In this work, we adopt for the parameters above the values given in Table 1.

In order to model the time variability, we assumed large velocity variations such that the maximum velocity change is $\Delta v \sim v_j$ with intermediate and long periods ($\tau \geq R_j/c_a > \tau_{\rm dy} = R_j/v_j$). The jet injection velocity at the inlet is varied according to a "periodic" step function, so that the jet is periodically "turned on" with a supersonic velocity $v_{\rm on}$ for a period $\tau_{\rm on}$, and periodically "turned off" to a small velocity $v_{\rm off}$ for a period $\tau_{\rm off}$. The velocity change is then, $\Delta v = v_{\rm on} - v_{\rm off} \simeq v_{\rm on}$ which we identify with v_j, that is, $v_{\rm on} \equiv v_j$. This is consistent with observations which indicate that the amplitude of the radial velocity variations in the emission knots can be very large (e.g., in the HH 46/47 jet) and the knot shock speed can be greater than 100 km s^{-1} (Reipurth 1989a). The multiple bow shock structures that move into the wakes of previous ejections, as in HH 111, are also expected to be produced by large-amplitude velocity variations. If both the internal knots and the multiple bow shocks are a product of episodic accretion events, as we are assuming here, then massive ejections along the stellar jets could be produced every 100–1000 yr (e.g., HR; Hartmann et al. 1993). So, for the period of variability, we take values which range from few to many times the dynamical timescale of the jet [$\tau \simeq (6$–$40)\tau_{\rm dy}$], corresponding to a few hundred years. These values are representative and are not intended to fit any particular system. Other choices are possible; for example, SN chose to model systems with smaller amplitude and higher frequency velocity variations.

3. THE SIMULATIONS

The values of the parameters of our simulations are listed in Table 1. The first model (I) describes the evolution of an $\eta = 10$

TABLE 1

VALUES OF PARAMETERS USED IN MODELS

Model	n_a (cm^{-3})	T_a (K)	R_j (cm)	M_j	η	q_{bs}[a]	q_{js}	τ_{on}/τ_{dy}	τ_{off}/τ_{dy}
I.....	1000	9×10^4	2×10^{16}	9.5	10.0	7×10^{-3}	9×10^{-2}[b]	3.0	3.0
II.....	60	3×10^4	10^{16}	30	3.0	15	0.56[c]	22.5	17.3

[a] Estimated using eq. (7), Paper I.
[b] Estimated using eq. (2.13), Falle & Raga 1993.
[c] Estimated using eq. (8), Paper I.

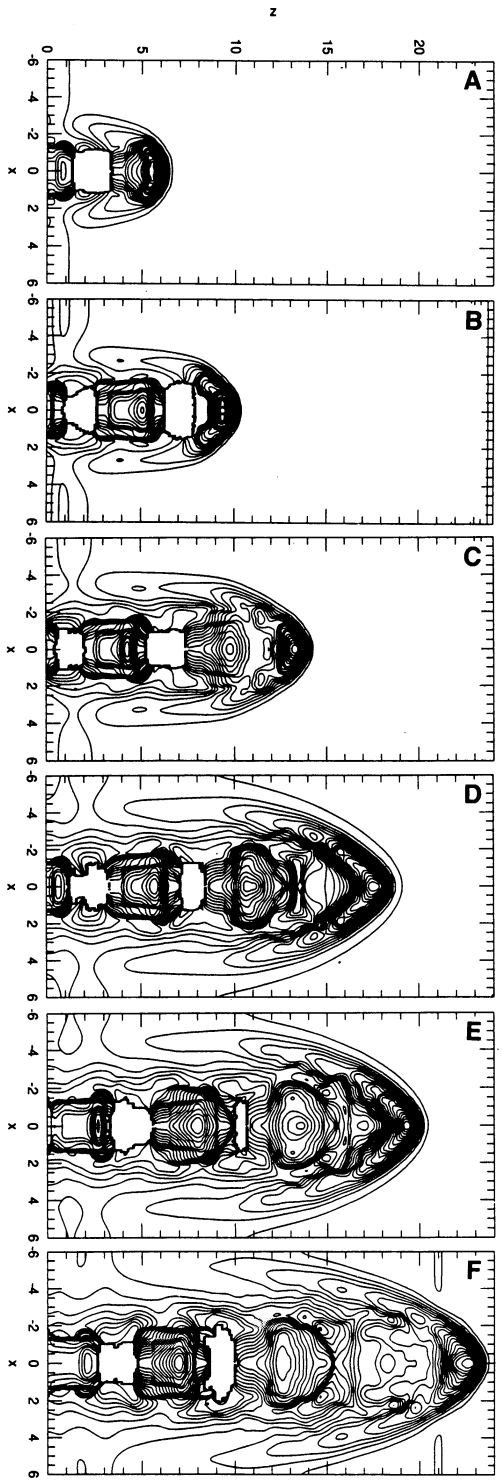

cooling jet subject to high-amplitude velocity perturbations of intermediate period. The second model (II) describes the evolution of an $\eta = 3$ cooling jet subject to high-amplitude velocity perturbations of long period. Subsections 3.1 and 3.2 present the results of the first and second calculations, respectively.

3.1. *The Evolution of a Jet with Intermediate-Period Velocity Variations*

Figure 1 depicts the time evolution of the central density contours of an intermittent jet periodically "turned on" with a supersonic velocity $v_j = 150$ km s^{-1} and periodically "turned off" with a subsonic velocity 15 km s^{-1}. The "turning on" and quiescent periods in this case are both given by $\tau_{on} = \tau_{off} = (R_j/c_a) \simeq 127$ yr, corresponding to a total period $\tau \simeq 254$ yr. Compared to the jet dynamical time scale $\tau_{dy} = R_j/v_j$, $\tau_{on} = \tau_{off} = 3\tau_{dy}$. The initial input parameters are (see model I, Table 1) $\eta = 10$, $n_a = 1000$ cm^{-3}, $R_j = 2 \times 10^{16}$ cm, $M_j = 9.5$ (corresponding to $M_a = 3$), and $T_j = T_a/\eta = 9090$ K. The entire evolution displayed in Figure 1 corresponds to $t \simeq 1387$ yr (or $11R_j/c_a$). The initial value of the cooling distance parameter for the leading bow shock at the jet head is given by $q_{bs} \simeq 7 \times 10^{-3}$, corresponding to a bow shock velocity $v_{bs} \simeq 114$ km s^{-1} (see eqs. [2] and [7] of Paper I). The jet shock (or Mach disk), for which $v_{js} \simeq v_j - v_{bs} \simeq 36$ km s^{-1}, has a cooling length parameter $q_{js} \simeq 0.31\ [(n_j/1000)\ \text{cm}^{-3}]^{-1}[(v_j/45)\ \text{km s}^{-1}]^{-4.7}[R_j/(2 \times 10^{16})\ \text{cm}]^{-1} \simeq 9 \times 10^{-2}$ (evaluated from eq. [2.13] of Falle & Raga 1993, which is valid for shock velocities $v_s < 90$ km s^{-1}). These values imply that both shocks in the jet head cool very fast ($q_{bs}, q_{js} \ll 1$) and are, therefore, nearly isothermal. The cold shell formed in the jet head is thus very thin (as shown in Fig. 1) and the head itself resembles a bullet of dense gas moving through the ambient medium (see also Fig. 6 of Paper I).

The parcels of supersonic flow which are injected every 254 yr (and keep flowing for half a period of 127 yr) are clearly evident. In each time interval of Figure 1, a new parcel emerges from the jet inlet (except in Figs. 1*e* and 1*f* which show the same emerging parcel). They cause the formation of pulses which quickly evolve to a chain of shock structures. Figure 2*a* gives a closer view of the last snapshot of Figure 1, that is, at $t \simeq 1387$ yr. Figure 2*b* shows the corresponding velocity distribution map at that time. As the shocks propagate downstream, they tend to widen and weaken. The number of internal shock structures formed along the outflow ($z_{max} = 24R_j$) is in agreement with the number expected from equation

FIG. 1.—The midplane density contours evolution of an intermittent cooling jet with intermediate period of variability [$\tau_{on} = \tau_{off} = 3(R_j/v_j) \simeq 127$ yr], and initial parameters $\eta = 10$, $n_a = 1000$ cm^{-3}, $R_j = 2 \times 10^{16}$ cm, $v_j = 150$ km s^{-1}, $M_j = 9.5$, and $M_a = 3$ (model I of Table 1). The z- and x-coordinates are in units of R_j. The contour lines are separated by a factor of 1.2, and the density scale covers the range from $\simeq 0.01$ up to $65/n_a$. The times depicted are (in units of $R_j/c_a = 127$ yr): (*a*) 2.4; (*b*) 4.1; (*c*) 5.9; (*d*) 8.3; (*e*) 9.2; and (*f*) 11.0

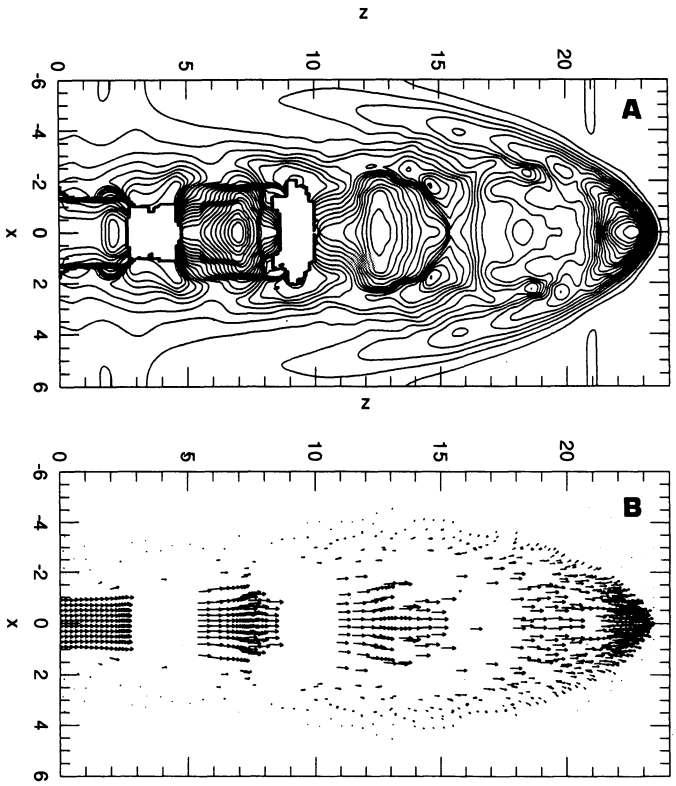

FIG. 2.—A closer view of the last snapshot of Fig. 1 at $t \simeq 11(R_j/c_a) \simeq 1387$ yr. (Fig. 2*a*) shows the central density contour, and Fig. 2*b*, the corresponding velocity distribution map within $y = \pm 0.3R_j$

(1) ($N_{IS} \simeq 4$). During the subsonic phases, the jet beam is starved of material, producing "gaps" between the supersonic parcels. We note also that constant interaction with the evolving internal peaks causes the head of the jet to have a structure which differs significantly from that of a steady jet (see Fig. 6 of Paper I).

Each internal supersonic parcel develops a pair of shocks: a forward (downstream) shock which sweeps up the low-velocity, diffuse material ahead of the perturbation and propagates downstream in the jet with a velocity v_{is}; and a reverse (upstream) shock which decelerates the high-velocity material in the perturbation and propagates with a velocity $v_{rs} \simeq v_j - v_{is}$. In order to illustrate in more detail how the discontinuities of the jet in Figure 1 evolve, Figure 3 shows the axial density along the symmetry axis ($x = y = 0$) for the six snapshots shown in Figure 1. (The axial pressure has a similar evolutionary behavior.) The density evolution of the leading working surface at the head of the jet is also depicted. We find that for each internal shock structure a density peak develops between the two shocks. Due to the long period of the velocity variations, the peaks do not interact and remain separated by the rarefied material injected in the subsonic phase. As the peaks travel downstream, they widen and fade and eventually disappear close to the leading working surface. These effects are due to the increase in the pressure of the postshock gas which causes both the separation between each pair of shocks and the expulsion of jet material laterally to the cocoon and to the rarefied portions of the beam itself.

The lateral widening and fading of the internal shocks is highlighted in Figure 4 which illustrates the density (*solid lines*) and pressure (*dashed lines*) across the flow as a function of the distance from the source at $t \simeq 1387$ yr (or $11R_j/c_a$) for the four internal shock structures of Figures 1*f* and 3*f*. The high pressure and density of the leading working surface have been clipped in the figure in order to highlight the lower level features of the internal outflow. As the internal shock structures propagate downstream, the pressure in the postshock medium pushes the material to the cocoon that surrounds the beam. As a consequence, the density and pressure of the shocked material decrease. This result is in agreement with the results of SN. We note that the density and pressure are very low in the cocoon. Thus the undersampling of the cocoon by the SPH particles is acceptable, since the cocoon has little dynamical effect. The material which the internal shocks push into the cocoon produces wakes that can be seen in Figure 1 and gives some of these structures the appearance of internal bow shocks. This effect has been predicted by Raga et al. (1990) and is also clearly evident in the two-dimensional maps of SN.

Figure 5 shows the position as a function of time of the leading working surface and the internal shock structures along the symmetry axis of the jet. The shocks labeled with numbers 6 and 7 have emerged from the jet inlet after $t = 12R_j/c_a = 1524$ yr when the leading working surface had already left the computation domain.

The internal shocks move downstream with an average velocity $v_{is}/c_a \simeq 2.7$, or in other words, with nearly the jet velocity in the supersonic phase $v_u \simeq v_j = 3c_a = 150$ km s^{-1}. This result is in agreement with equations (3) and (4) for a density ratio of the fast high density material (upstream of the supersonic discontinuity) to the low-density material (downstream of the discontinuity) $\rho_u/\rho_d \gg 1$, as is the case (see § 2.1). We note that in the present study, due to the high density ratio between the fast and the slow portions of the flow, the propagation velocity of the forward shock, which is of the order of v_j, is much larger than that of the reverse shock $v_{rs} \simeq 0$ (see eq. [3]). So, the forward shock is much stronger than the reverse shock. Similar behavior occurs in the bullet models (Norman & Silk 1979) and has been detected in one of the one-dimensional models investigated by HR in which the velocity perturbations are accompanied by similar density enhancements. The domination of the strong forward shock implies that line emission occurs in a single peak behind this shock.

Figure 5 also indicates that the average propagation velocity of the leading bow shock at the head of the jet is smaller than the velocity of the internal shocks and is initially in rough agreement with the value estimated from equation (2) of Paper I ($v_{ws}/c_a \simeq 2.2$). The variations in the propagation velocity of the leading working surface indicated by the figure between $t/127$ yr $\simeq$ 7–9 (which result in a minimum propagation velocity $v_{ws}/c_a \simeq 0.9$ at $t/127 \simeq 8.3$) are caused by a global thermal instability in the leading bow shock. This effect has been studied in detail in Paper I. High-velocity radiative shocks, when subject to small variations in their shock velocity, oscillate between radiative and nearly adiabatic shock phases. Accompanying these variations in the shock velocity are oscillations in the density and pressure of the shocked material. These oscillations are clearly evident in Figure 6 which depicts the time evolution of the axial density (Fig. 6*a*) and pressure (Fig. 6*b*) of the shocked cooled material at the head of the jet (labeled ws). The maximum of the density and pressure oscillations corresponds to the radiative jet shock phase, while the minimum of the oscillations correspond to the nearly adiabatic jet shock phase (see Paper I).

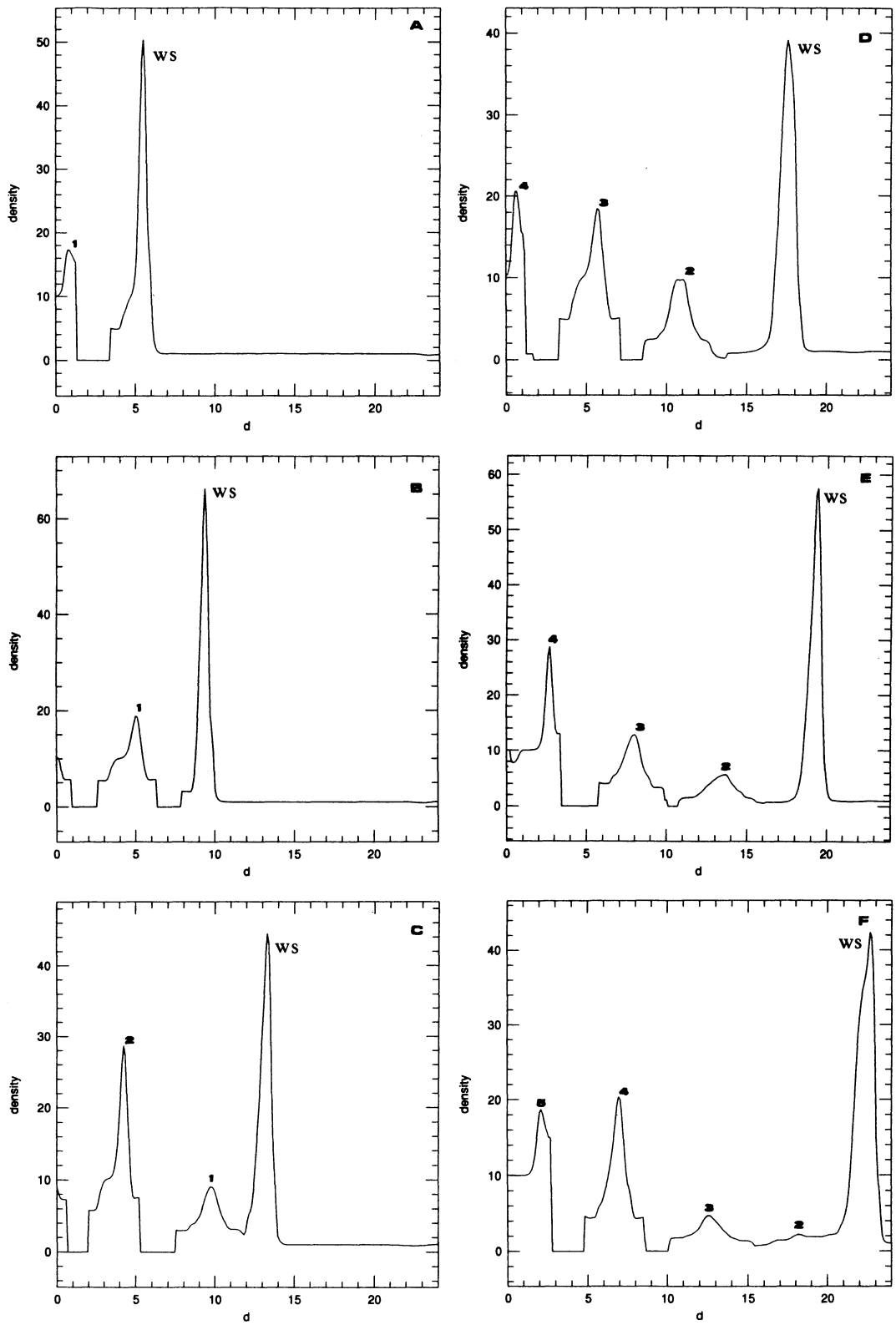

FIG. 3.—The axial density along the symmetry axis ($x = 0 = y$) of the jet for the six snapshots shown in Fig. 1. The peak corresponding to the leading working surface at the head of the jet is labeled "ws." The internal shocks are labeled with numbers which increase according to the order of appearance of each shock. The density and the distance d along the z-axis are scaled with the values $n_a = 1000\,\mathrm{cm}^{-3}$ and $R_j = 2 \times 10^{16}$ cm, respectively.

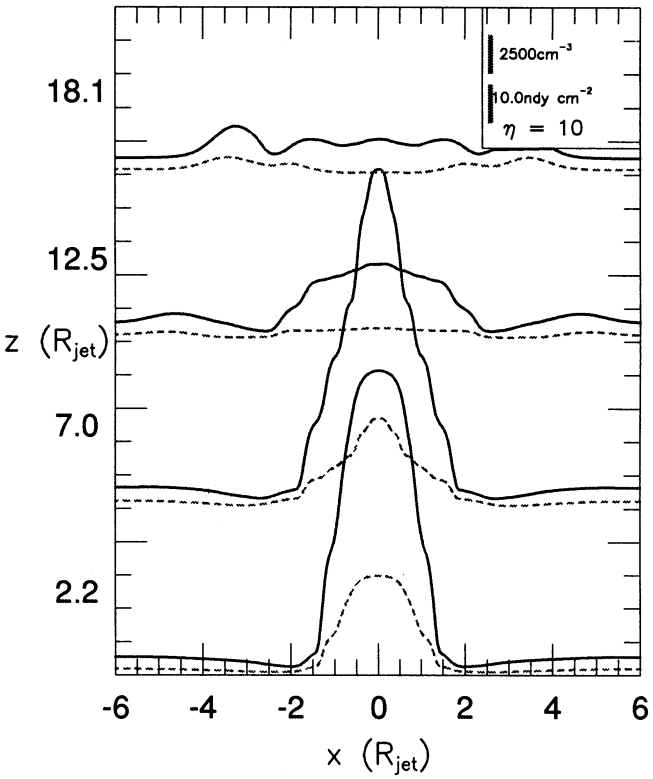

FIG. 4.—The density (*solid lines*) and pressure (*dashed lines*) across the flow (of the central slice) as a function of the distance along the jet of Fig. 1 at $t \simeq 11(R_j/c_a) \simeq 1387$ yr. The four positions depicted correspond to the four internal shocks of Figs. 1*f* and 3*f*. The pressure and density of the leading working surface are very high and have been clipped in the figure in order to highlight the lower level features of the internal outflow. The vertical scales can be calibrated using the markers in the top right corner.

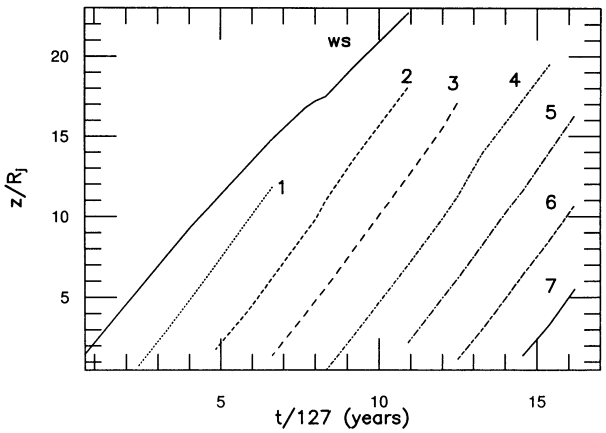

FIG. 5.—The position of the leading bow shock (labeled ws) and the internal shocks at the symmetry axis of the jet as a function of time. The position and time are in units of R_j and $R_j/c_a = 127$ yr, respectively. The shocks labeled with numbers 6 and 7 have emerged in the jet inlet after $t = 12R_j/c_a = 1524$ yr when the leading working surface had already left the top of computation domain at $z_{max} = 24R_j$.

Figure 6 also shows the density and pressure evolution of the internal knots along the axis of the jet. Due to their short lifetime compared to the leading working surface, we do not detect any evidence of density and pressure oscillations in these internal shocks. Figure 6 shows that all internal shocks fade after $\sim(5\text{–}6)R_j/c_a$, which is of the order of one-half the period of the oscillations of the leading working surface. The strong cooling in the postshock gas keeps the internal shocks effectively isothermal. As a consequence, they produce large compressions and low postshock temperatures ($T \simeq 10^4$ K) before they vanish. Figure 6*a* indicates that the maximum density contrast across the internal shocks is $n_{is}/n_a \simeq 30$, while the maximum density contrast at the leading working surface is $n_{ws}/n_a \simeq 65$. This implies that the emission from internal shocks is of smaller intensity and excitation than the emission from the head, in agreement with the observations. Adiabatic pulsating jets show smaller compression ratios in the internal shocks (Wilson 1984).

3.2. *The Evolution of an Intermittent Jet with Long-Period Velocity Variations*

Figure 7 depicts the central density evolution and the corresponding velocity distribution of an overdense cooling jet with a long-period variability. The input parameters of this simulation (model II) are given in Table 1. This simulation has been particularly motivated by the observations of such systems as HH 111, which shows evidence of two bow shocks separated

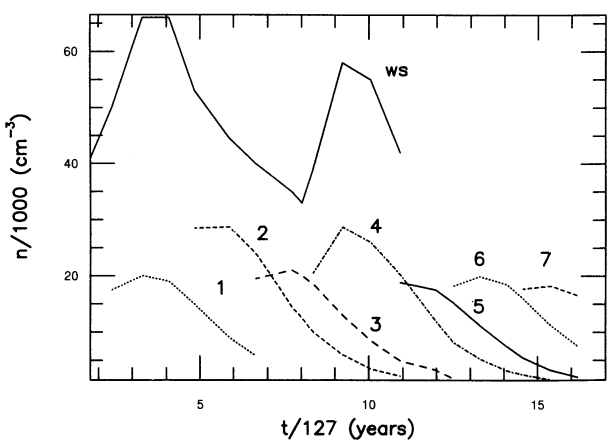

FIG. 6*a*

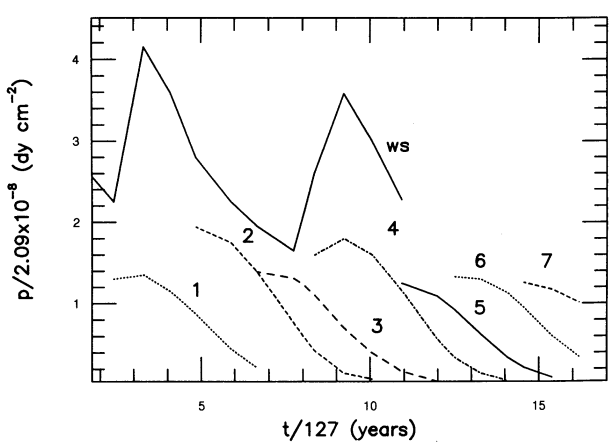

FIG. 6*b*

FIG. 6.—(*a*) The density (n) and (*b*) pressure (p) evolution of the internal knots along the axis of the jet of Fig. 1. The time interval depicted is the same as Fig. 5. It is given in units of $R_j/c_a = 127$ yr

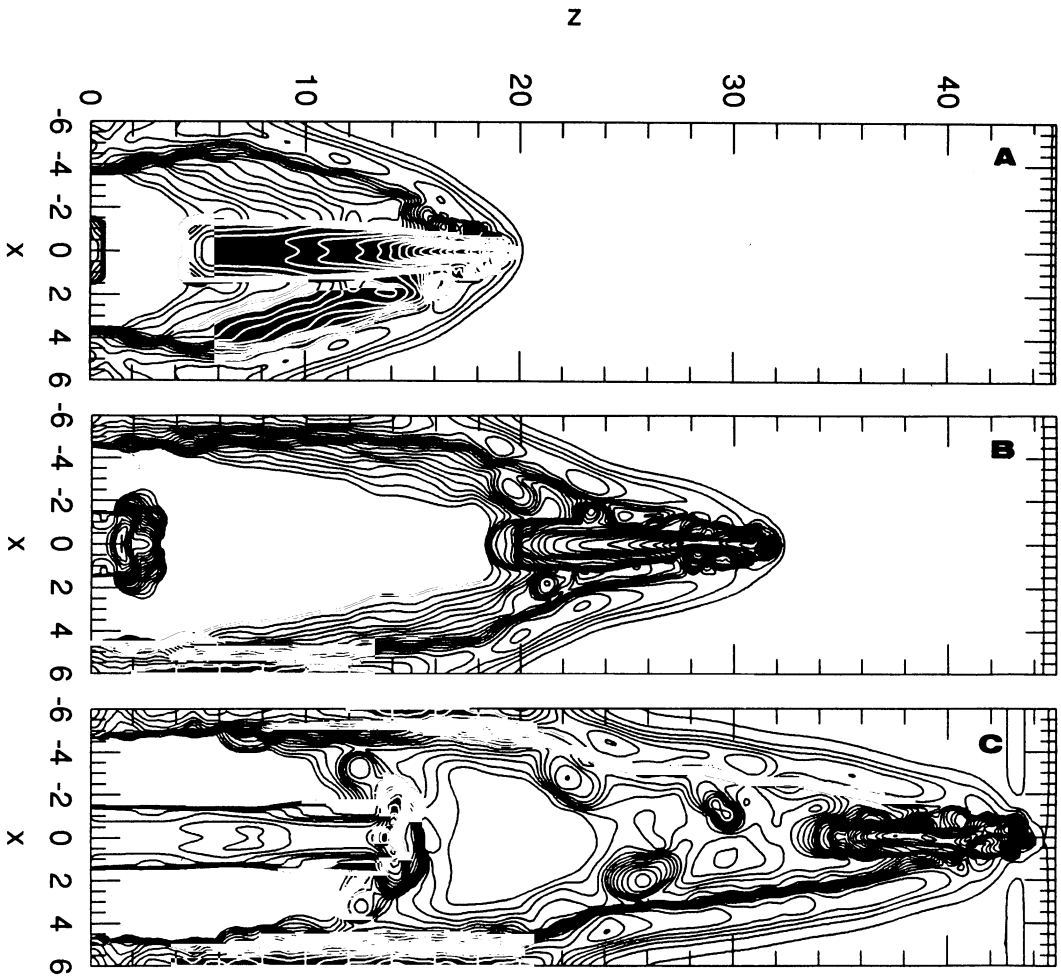

FIG. 7.—The midplane density contours evolution and the corresponding velocity distribution of an intermittent cooling jet with a long period variability ($\tau_{on} = 22.5\tau_{dy} = 143$ yr, and $\tau_{off} = 17.3\tau_{dy} = 110$ yr) and input parameters $\eta = 3$, $n_a = 60$ cm^{-3}, $R_j = 10^{16}$ cm, $v_j = 500$ km s^{-1}, $M_j = 30$, and $M_a = 17.3$ (model II of Table 1). The z- and x-coordinates are in units of R_j. The density contour lines are separated by a factor of 1.2 and the density scale covers the range from $\simeq 0.12$ up to $1130/n_a$. The minimum velocity in the velocity map is $\simeq 10^{-6} c_a$ and the maximum velocity is $\simeq 20 c_a$, with $c_a = 29$ km s^{-1}. The times depicted are (in units of $R_j/c_a = 110$ yr) as follows: (*a*) 1.6; (*b*) 2.5; and (*c*) 3.4

by many jet radii on each side of the source, moving away from the source, and leaving only a faint and diffuse trail of gas. These observations suggest that if the multiple bow shocks are due to multiple outflow episodes from the source then they could correspond to long-period velocity variations like the one presented in Figure 7.

The jet in Figure 7 was initially "turned on" with a supersonic velocity $v_j = 500$ km s^{-1} (which corresponds to a jet Mach number $M_j = 30$ and an ambient Mach number $M_a = 17.3$) for a period τ_{on} which was much greater than the dynamical timescale of the jet ($\tau_{dy} = R_j/v_j$): $\tau_{on} = 1.3(R_j/c_a) = 22.5\tau_{dy} = 143$ yr (for $R_j = 10^{16}$ cm). It was then turned off for a period $\tau_{off} = 1(R_j/c_a) = 110$ yr to a "quiescent" phase with a weakly supersonic velocity of 19 km s^{-1} ($M_j = 1.7$). After that period, the jet was returned to the highly supersonic phase in which it continued until the end of the calculation $t \simeq 3.4(R_j/c_a) \simeq 587(R_j/v_j) \simeq 374$ yr. Only one internal working surface developed over the whole space domain of the computation ($z_{max} \simeq 45R_j$). This result is consistent with equation (1) which predicts a number of internal working surfaces $N_{is} \simeq 1$ for this case. Figure 7*a* depicts the evolution of the first highly supersonic parcel that gave origin to the leading working surface. Figure 7*b* shows the second fast parcel emerging on the trail of diffuse gas formed behind the first parcel during the slow, quiescent phase. In Figure 7*c*, the second supersonic parcel has developed an internal working surface with a bow shock structure. The evolution of the jet before the time sequence illustrated in the figure is very similar to the evolution of the jet of Figure 4 of Paper I which has similar input parameters. For this reason, we do not present its early evolution here.

The input parameters (see Table 1) correspond to an initial cooling length parameter for the leading bow shock at the head of the jet $q_{bs} \simeq 15$ and an initial bow shock velocity $v_{bs} \simeq 317$ km s^{-1} (see eqs. [2] and [7] of Paper I). The leading jet shock has an initial cooling length parameter $q_{js} \simeq q_{bs}\eta^{-3} \simeq 0.56$ (see eq. [8] of Paper I) and a jet shock velocity $v_{js} \simeq v_j - v_{bs} \simeq 183$ km s^{-1}. These values imply that the shocked ambient material at the jet head is essentially adiabatic ($q_{bs} \gg 1$) while the shocked jet material is radiative ($q_{js} < 1$). Thus, the gas that has accumulated at the head of the jet forming a dense shell of cold material consists of the shock-heated *jet* material that has cooled by radiation. We note from Figure 7 that the shell at the head of the jet is clumpy and irregular. This structure is very

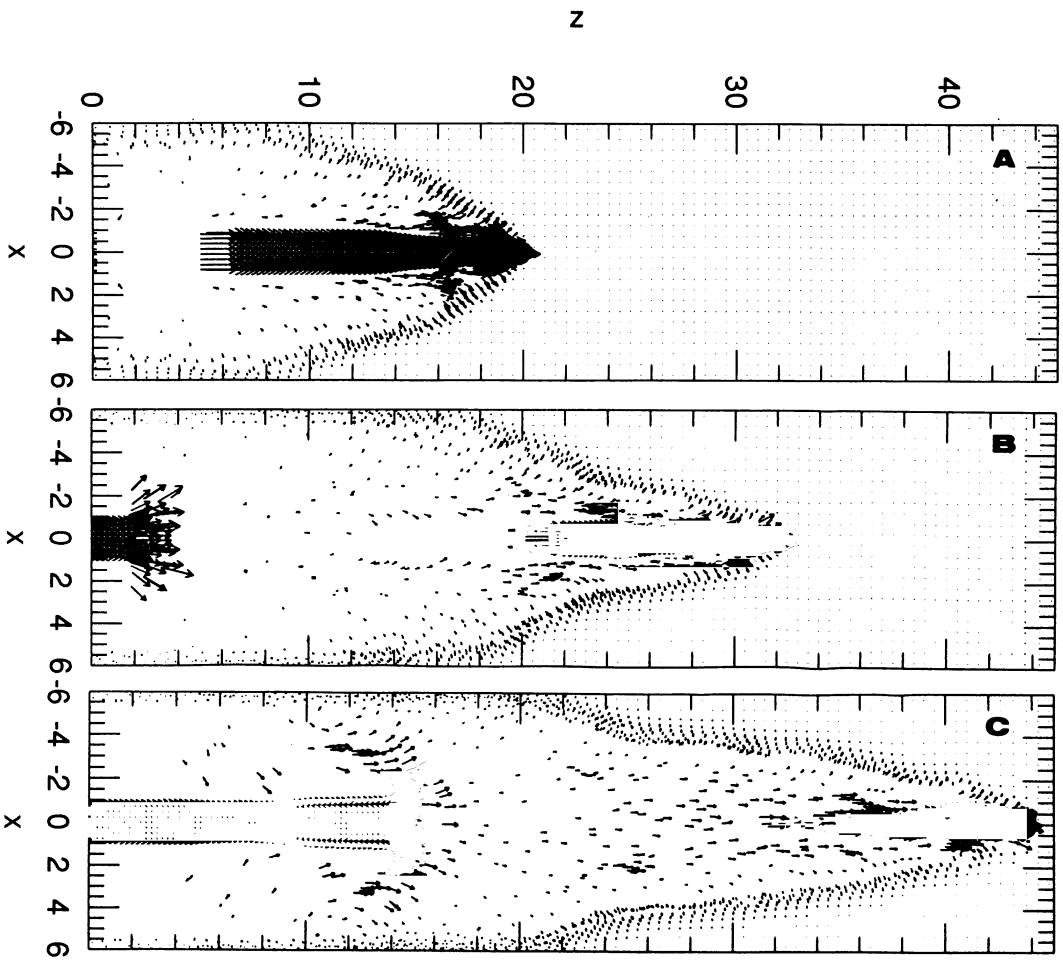

FIG. 7—*Continued*

similar to those found in three-dimensional simulations of steady jets (see, for example, Fig. 4 of Paper I) and occurs because the dense shell becomes dynamically unstable to the Rayleigh-Taylor instability. Part of these pieces into which the shell breaks spill out to the cocoon forming, together with the shell, an elongated narrow plug of cold gas in the head as shown in Figure 7 (see Paper I for more details).

The velocity of propagation of the leading bow shock increased with time. This acceleration is directly related to the narrowing of the jet beam at the head and is common with steady jets (e.g., Paper I). According to equation (2) of Paper I, the velocity of the leading bow shock is given by $v_{bs} \simeq v_j[1 + (\eta\alpha)^{-1/2}]^{-1}$, where $\alpha = (R_j/R_h)^2$ is the ratio between the radius of the jet beam and the radius of the jet head. In Figure 7, the velocity of the leading bow shock is initially given by $v_{bs} \simeq 317$ km s^{-1} and is consistent with the equation above with $\alpha = 1$. At the end of the integration, in Figure 7*c*, α has increased to $\alpha \simeq 4$ and $v_{bs} \simeq 412$ km s^{-1}, in fair agreement with the prediction.

A cavity is formed behind the first supersonic parcel during the "quiescent" phase (Fig. 7*b*). Later, it is partially filled by jet material injected in the second highly supersonic phase (which also pushes the low-velocity gas injected in the earlier quiescent phase) and by material of the cocoon, which is composed of the remnants of the dense shell of the head. The three little blobs seen between $z = 20$ and $30R_j$ in Figure 7*c* are local density concentrations that were part of these remnants.

During the quiescent phase, jet material is injected in the inlet at a low but weakly supersonic velocity ($M_j = 1.7$). It thus develops a very weak shock as it propagates downstream on the diffuse trail left by the first highly supersonic parcel. This shock front is then overtaken by the second highly supersonic parcel which starts to be ejected at $t = 2.3R_j/c_a \simeq 253$ yr. A double shock structure (see Fig. 7*c*), similar to the one at the leading working surface, quickly develops. A forward bow-shaped shock is formed as the parcel sweeps up the low-velocity material ahead of it and a reverse weaker shock is formed when the supersonic material coming behind is decelerated at the discontinuity. (Eventually, a triple shock structure can be seen on the plots of the axial pressure. The triple shock is a consequence of the superposition of the weak shock associated with the slow phase and the double shock that originated with the injection of the second highly supersonic parcel.) The propagation velocity of this internal working surface (which corresponds to the internal bow shock speed) is initially given by $v_{is} \simeq 383$ km s^{-1} which corresponds approximately to the value predicted by equation (3) for a density ratio $\beta^2 \simeq \eta = 3$, which is appropriate since the slow material has adjusted to a density close to that of the ambient gas. This internal working surface experiences some acceleration as it propagates down-

stream through the cavity behind the leading parcel. By the time depicted in Figure 7*c*, the propagation velocity has increased to a value close to the jet velocity $v_{is} \simeq 500$ km s^{-1}, and the corresponding reverse shock velocity has decreased to $v_{rs} \simeq v_j - v_{is} \simeq 0$. Later, the velocity of the internal working surface decreases again as it finds increasing resistance of the material of the tail behind the leading working surface.

As in Figure 1 (see also Figs. 4 and 5 of Paper I), the density of the shell of the leading working surface varies with time as the radiative shock becomes thermally unstable (see Paper I). The density in the z-axis varies from $\simeq 1070/n_a$ (in Fig. 7*a*) to $\simeq 1110/n_a$ (in Fig. 7*b*) and fades to $\simeq 950/n_a$ (in Fig. 7*c*). The corresponding temperature of the cold shell is $T \simeq 10^4$ K.

The internal working surface which on the average propagates faster than the leading working surface has a weaker shock structure. The reverse (upstream) shock is more radiative than the forward (downstream) shock. This shock-heated material then cools and forms a cold shell whose maximum density on the axis remains approximately constant over the time interval depicted in Figures 7*b* and 7*c*, with an average value $\simeq 6.8n_a$, corresponding to a temperature $T \simeq 1.4 \times 10^4$ K. In Figure 7*b*, the axial density of the postshock cold material is 426 cm^{-3}, and in Figure 7*c*, it is 435 cm^{-3}. This result is consistent with the expectation that the emission of the internal working surface will be of lower intensity and excitation than that of the leading working surface, as required by most observations. Later, when the leading working surface has left the domain of integration, the density of the material of the secondary working surface increases to $\simeq 10n_a$. Unlike the case of the internal knots formed with small period variability (Fig. 1), no fading of the internal working surface has been detected with long period variability. Figure 7*c* also shows that the beam associated with the second working surface experiences some collimation caused by the high-pressure, shock-heated ambient gas that had been deposited in the cocoon surrounding the beam. This collimation pinches the beam and drives a weak internal shock at $z \simeq 3R_j$.

It is interesting to note that the separation between the two working surfaces in Figure 7*c*, $\sim 29.5R_j = 2.95 \times 10^{17}$ cm, is consistent, for example, with the separation between the two pairs of bow shocks observed on both sides of the HH 111 jet: the western pair (bow shocks P and V) has a separation of $\sim 5 \times 10^{17}$ cm and the eastern pair (bow shocks X and Y) has a separation $\sim 1.8 \times 10^7$ cm; Reipurth (1989b). Our model is also consistent with the observed higher intensity and excitation of the leading bow shock structure of the western jet relative to the internal bow shock. Of course, the input parameters do not match this particular jet system exactly; our results agree only qualitatively with the observations.

4. DISCUSSION AND CONCLUSIONS

In this work, we have presented fully three-dimensional hydrodynamical simulations of overdense, radiative cooling, intermittent jets with high-amplitude velocity variations ($\Delta v \simeq v_j$) of intermediate ($\tau \simeq \tau_{dy} = R_j/v_j$) and long ($\tau \gg \tau_{dy}$) variability periods. These simulations are qualitatively in agreement with the observed emission knots of protostellar jets ($\tau \simeq \tau_{dy}$) or with the observed multiple bow shock structures separated by long trails of diffuse gas ($\tau \gg \tau_{dy}$). However, our simplified treatment of the radiative cooling of the gas prevents us from performing a detailed comparison of our models with the radiation from observed protostellar jets. In particular, the density contour maps presented here while describing reasonably well the expected gas distribution do not necessarily correspond to the observed emission-line images. For example, the elongated dense plugs that can eventually develop at the head of the jet (as in model II; see below) as a consequence of the disruption and spilling to the cocoon of the cold shell might not be seen in the images if the plug has become mostly neutral and therefore unable to strongly radiate. Nonetheless, with the help of the density contour maps, we can delineate the basic structural characteristics and dynamics of the protostellar jets.

We found that the high-amplitude supersonic velocity variations of intermediate period (model I) quickly evolve to form a chain of regularly spaced radiative shocks which have large proper motions, high radial velocities, and low intensity spectra. All these characteristics are in agreement with the observed properties of the knots of protostellar jets and have also been noted independently on the models of HR and the SN.

The number of internal shock structures that develop along the jet is roughly given by equation (1) which relates the dynamical timescale of the jet to the period of velocity variability. When a supersonic parcel impacts the slow rarefied material that has been injected in an earlier quiescent phase, a *forward* shock quickly forms (as it sweeps up the slow material) and propagates downstream at $v_{is} \simeq v_j$, the jet velocity in the highly supersonic phase. The velocity variations in our simulations are accompanied by high density contrasts between the fast and the slow portions of the flow. This causes the *reverse* shock (where the discontinuity decelerates the fast material coming from behind) to be much weaker than the *forward* shock (see § 3.1). As a consequence, the emission behind the discontinuity must be essentially single peaked, instead of double peaked as in the SN and some of the HR models that have assumed mass flux conservation. In those cases, the reverse shock is stronger and so is the emission behind it. Our internal shocks resemble the bullets modeled by Norman & Silk (1979).

The efficient radiative cooling of these internal shock structures causes them to become dense and cold. As they propagate away from the source, they widen and eventually fade close to the jet head. This is caused by the high pressure gradient developed in the postshock gas which pushes the material sideways to the cocoon and increases the separation between the pair of shocks that bound each density peak. Since the internal shock structures propagate at nearly the supersonic jet speed, they are weaker than the shock structure at the head of the jet. The maximum density behind the internal shocks is smaller than the maximum density of the cold shell at the head of the jet. This indicates that these internal shocks are of lower intensity and have lower excitation emission spectrum than the jet head, as required by the observations. Also, the widening and fading of the internal shocks as they propagate downstream implies that knots must be more common close to the driving source. This result is also in agreement with the observations.

The larger amplitude of the velocity variations in our simulations compared to those of SN caused a steepening of the discontinuities into stronger shocks with higher postshock pressures much closer to the jet inlet than in their models. As a consequence, there is a more efficient explusion of the shocked material sideways to the cocoon which, in turn, causes a faster widening and fading of the knots. Also, due to the longer period of the velocity variations compared to the SN models,

the internal shock structures in our simulations remain independent of one another.

In the case of the long period velocity variability (model II), our simulations have produced a pair of bow-shaped working surfaces separated by a long trail of very diffuse gas found in systems like the HH 111 jet. A leading working surface develops at the head of the jet when the first highly supersonic portion of flow is injected into the ambient medium. Contrary to the jet of model I (whose head structure is modified by interactions with the internal knots), the head structure of the jet of model II is very similar to that of steady jets (Paper I). A dense shell is formed by the radiative cooling of the shock-heated jet gas. As in steady jets, the shell disrupts into pieces which resemble the knotty structure observed in many HH objects (e.g., HH 1, HH 2, HH 19, HH 12) (e.g., Böhm & Solf 1985; Strom, Strom, & Stocke 1983; Mundt et al. 1984). The shell also suffers density variations with time which are due to the development of global thermal instabilities of the radiative shock. As we have argued in Paper I, such density variations may have important effects on the emission pattern of the HH objects and may explain, in particular, the brightness variability that is sometimes observed. After the disruption, parts of the clumpy shell spill out to the cocoon forming, with the shell, an extended plug. The narrowing of the jet beam at the head causes some acceleration of the jet system.

After the quiescent phase (which follows the injection of the first supersonic portion of flow) in which the jet material is injected at a low velocity, a second portion of highly supersonic flow is introduced in the system and develops a second working surface which propagates down the flow. A trail of very diffuse gas separates both working surfaces by many jet radii, in agreement with the observations of, for example, the HH 111 and HH 47 jets. This second working surface has a double shock structure similar to that in the leading working surface: a forward bow-shaped shock is formed as the low-velocity material is swept up, and a weaker reverse shock is formed when the supersonic material coming from behind is decelerated at the discontinuity. The initial velocity of propagation of this working surface is smaller than the jet injection speed, but the beam accelerates as it propagates downstream through the cavity behind the leading working surface, and the velocity increases close to the jet injection speed. Later, as the working surface encounters the increasing resistance of the material of the wakes behind the leading working surface, its velocity decreases again.

The postshock radiative material also cools and forms a cold shell in this second working surface whose density is much smaller than that of the shell of the leading working surface. This result is consistent with the observation that the emission of the internal working surface is of lower intensity and excitation than that of the leading working surface.

Of course, since we did not choose input parameters that exactly match particular jet systems, our results agree only qualitatively with the observations. By adjusting the amplitude and period of the velocity variations, models might be generated which fit the morphology of the knots and multiple bow shock structures of protostellar jets.

It is well known that many young stellar objects are associated not only to the highly collimated, fast optical jets investigated in this work, but also to less-collimated, slower molecular outflows detected at radio wavelengths (e.g., Rodríguez 1989). Several authors have recently explored models in which the molecular outflows are driven solely by the collimated jets (e.g., Lizano et al. 1988; Stahler 1993; Masson & Chernin 1993; Raga & Cabrit 1993; Raga et al. 1993; Paper II). In Paper II, where we have investigated the momentum transfer process between steady state jets and the environment, the three-dimensional simulations indicate that the protostellar jets primarily transfer momentum to the ambient medium at the working surface. In particular, we have found that the observed extremely high velocity (EHV) CO features of the molecular outflows (which may also appear associated to H_2 emission knots, e.g., Bachiller et al. 1990) can be formed in the swept-up postshock gas at the bow shock. On the other hand, Raga & Cabrit (1993) have proposed that the molecular emission could be identified with the swept-up environmental gas that fills the cavity formed behind the internal working surfaces of a time-dependent ejected jet. In the case of the jet with intermediate variability period studied in the present work (model I), there is no evidence that the ambient material pushed aside by the internal bow shocks has had time to fill the cavities behind them (see Figs. 1 and 2). The swept-up ambient material cools at the edge of the cavities. But, our jet with long variability period (model II, Fig. 7) clearly shows that the ambient gas swept up by the leading working surface eventually refills the cavity formed behind it, in agreement with Raga & Cabrit's model. Also, Raga et al. (1993) explored a model in which the molecular outflows correspond to the turbulent envelopes of mixed jet and ambient material developed around time-dependent jets. This scenario is believed to be more appropriate for the case of very evolved outflow systems. According to the observations, the molecular gas can typically extend over transverse sizes which are about 20 times wider than the jet diameter. Our results for the evolved system of model II (Fig. 7) indicate that the envelope does not seem to much exceed about six jet diameters. However, this "narrowing" tendency of the distribution of the surrounding gas in our simulations can be partially due to the assumed periodic boundaries on y and x peripheries of the ambient box. Weak reflecting waves may develop on these boundaries on the late stages of evolution of a system causing some artificial colimation of the ambient envelope (see discussion in Paper I).

As in our previous investigations (Paper I, Paper II), in this study we have assumed a history-independent optically thin radiative cooling function to compute the losses of a fully ionized flow. By not following the history-dependent effects of nonequilibrium ionization of the gas or the transfer of ionizing radiation, we possibly underestimated the cooling rate in some parts of the postshock regions by as much as an order of magnitude (e.g., Innes et al. 1987). However, the inclusion of a detailed cooling evaluation, like the one performed in the one-dimensional calculations of HR, would require a substantial increase in computer power. Although future work should take into account those effects, we expect that the gross dynamical features obtained in the present analysis will not change. This expectation is supported by the comparison of our results (see also Paper I) with the calculations of SN (see also their recent calculations for steady flows; Stone & Norman 1993b), which included a nonequilibrium time-dependent cooling.

Finally, other possible origins of the internal shocks in protostellar jets could be the entrainment of ambient material surrounding the jet or the interaction of the beam with an inhomogeneous preshock medium. The first of these processes seems to play a secondary role in protostellar jets. In the numerical investigation of the momentum transfer processes

between steady state cooling jets and the ambient medium (Paper II), we found that the entrainment of ambient gas along the jet beam is important only in low Mach number ($M_j \leq 3$), low density ratio ($\eta \leq 3$) flows which, in general, is not the case for the typical protostellar jets for which $10 < M_j < 40$ and $\eta > 1$. The second possibility is examined in a forthcoming paper (Gouveia Dal Pino, Birkinshaw, & Benz 1994).

E. M. G. D. P. would like to acknowledge fruitful discussions with M. Birkinshaw, L. Chernin, and A. C. Raga. We are also very grateful to the referee for his relevant comments and suggestions. The simulations were performed on the Workstation HP Apollo 9000/720 of the Plasma Astrophysics Group of the Department of Astronomy of IAG/USP, whose purchase was made possible by the Brazilian agency FAPESP.

REFERENCES

Bachiller, R., Cernicharo, J., Martín-Pintado, J., Tafalla, M., & Lazareff, B. 1990, A&A, 231, 174
Benz, W. 1990, in Numerical Modeling of Stellar Pulsations: Problems and Prospects, ed. J. R. Buchler (Dordrecht: Kluwer), 269
———. 1991, in Late Stages of Stellar Evolution and Computational Methods in Astrophysical Hydrodynamics, ed. C. de Loore (Berlin: Springer-Verlag), 259
Birkinshaw, M. 1991, in Beams and Jets in Astrophysics, ed. P. A. Hughes (Cambridge: Cambridge Univ. Press), 278
Blondin, J. M., Fryxell, B. A., & Königl, A. 1990, ApJ, 360, 370 (BFK)
Böhm, K.-H., & Solf, J. 1985, ApJ, 294, 533
Chernin, L., Masson, C., Gouveia Dal Pino, E. M., & Benz, W. 1994, ApJ, 426, 204 (Paper II)
Dopita, M. A. 1978, ApJ, 37, 117
Falle, S. A. E. G., & Raga, A. C. 1993, MNRAS, 261, 573
Gouveia Dal Pino, E. M., & Benz, W. 1993a, ApJ, 410, 686 (Paper I)
———. 1993b, in Proc. of the Sub-Arcsecond Radio Astronomy Manchester Conference, ed. R. J. T. Davis & R. S. Booth (Cambridge: Cambridge Univ. Press), 375
———. 1993c, in Proc. of the IV International Toki Conference on Plasma Physics and Controlled Fusion, ed. T. D. Guyenne & J. J. Hunt (Paris: ESA), 333
Gouveia Dal Pino, E. M., Birkinshaw, M., & Benz, W. 1994, in preparation
Hartigan, P., & Raymond, J. 1992, ApJ, 409, 705 (HR)
Hartigan, P., Raymond, J., & Hartmann, L. 1987, ApJ, 316, 323
Hartigan, P., Raymond, J., & Meaburn, J. 1990, ApJ, 362, 624
Hartmann, L., Kenyon, S., & Hartigan, P. 1993, in Protostars and Planets III, ed. E. H. Levy & J. I. Lunine (Tucson: Univ. of Arizona Press), in press
Innes, D. E., Giddings, J. R., & Falle, S. A. E. G. 1987, MNRAS, 226, 67
Katz, J. 1989, Ph.D. thesis, Princeton Univ.
Kofman, L., & Raga, A. C. 1992, ApJ, 390, 359 (KR)
Lizano, S., et al. 1988, ApJ, 328, 763
Masson, C. R., & Chernin, L. 1993, ApJ, 414, 230
Morse, J. A., Hartigan, P., Cecil, G., Raymond, J. C., & Heathcote, S. 1992, ApJ, 339, 231
Morse, J. A., Heathcote, S., Cecil, G., Hartigan, P., & Raymond, J. C. 1993, ApJ, 410, 764
Mundt, R. 1988, in Proc. of NATO-ASI on Formation and Evolution of Low Mass Stars, ed. A. Dupree & M. T. V. T. Laga (Dordrecht: Reidel), 257
Mundt, R., Brügel, E. W., & Bührke, T. 1987, ApJ, 319, 275 (MBB)
Mundt, R., Bührke, T., Fried, J. W., Neckel, T., Sarcander, M., & Stocke, J. 1984, A&A, 140, 17
Norman, C. A., & Silk, J. 1979, ApJ, 228, 197
Raga, A. C. 1992, MNRAS, 258, 301
Raga, A. C., Cantó, J., Binette, L., & Calvet, N. 1990, ApJ, 364, 601
Raga, A. C., Cantó, J., Calvet, N., Rodríguez, L. F., & Torrelles, J. 1993, A&A, 276, 539
Raga, A. C., & Cabrit, S. 1993, A&A, 278, 267
Raga, A. C., & Kofman, L. 1992, ApJ, 386, 222 (RK)
Raga, A. C., & Noriega-Crespo, A. 1993, preprint
Rees, M. J. 1978, MNRAS, 184, 61P
Reipurth, B. 1985, A&A, 143, 435
———. 1989a, in Proc. of the ESO Workshop on Low Mass Star Formation and Pre-Main Sequence Objects, ed. B. Reipurth (Garching: ESO), 247
———. 1989b, Nature, 340, 42
Reipurth, B., Bally, J., Graham, J. A., Lane, A. P., & Zealey, W. J. 1986, A&A, 164, 51
Reipurth, B., & Heathcote, S. 1991, A&A, 246, 511
Reipurth, B., Raga, A. C., & Heathcote, S. 1992, ApJ, 392, 145
Rodríguez, L. F. 1989, Rev. Mexicana Astron. Af., 18, 45
Stahler, S. 1993, in Astrophysical Jets, ed. M. Livio, C. O'Dea, & D. Burgarella (Cambridge: Cambridge Univ. Press), 183
Stone, J. M., & Norman, M. L. 1993a, preprint (SN)
———. 1993b, preprint.
Strom, K. M., Strom, S. E., & Stocke, J. 1983, ApJ, 271, L23
Wilson, M. J. 1984, MNRAS, 209, 923

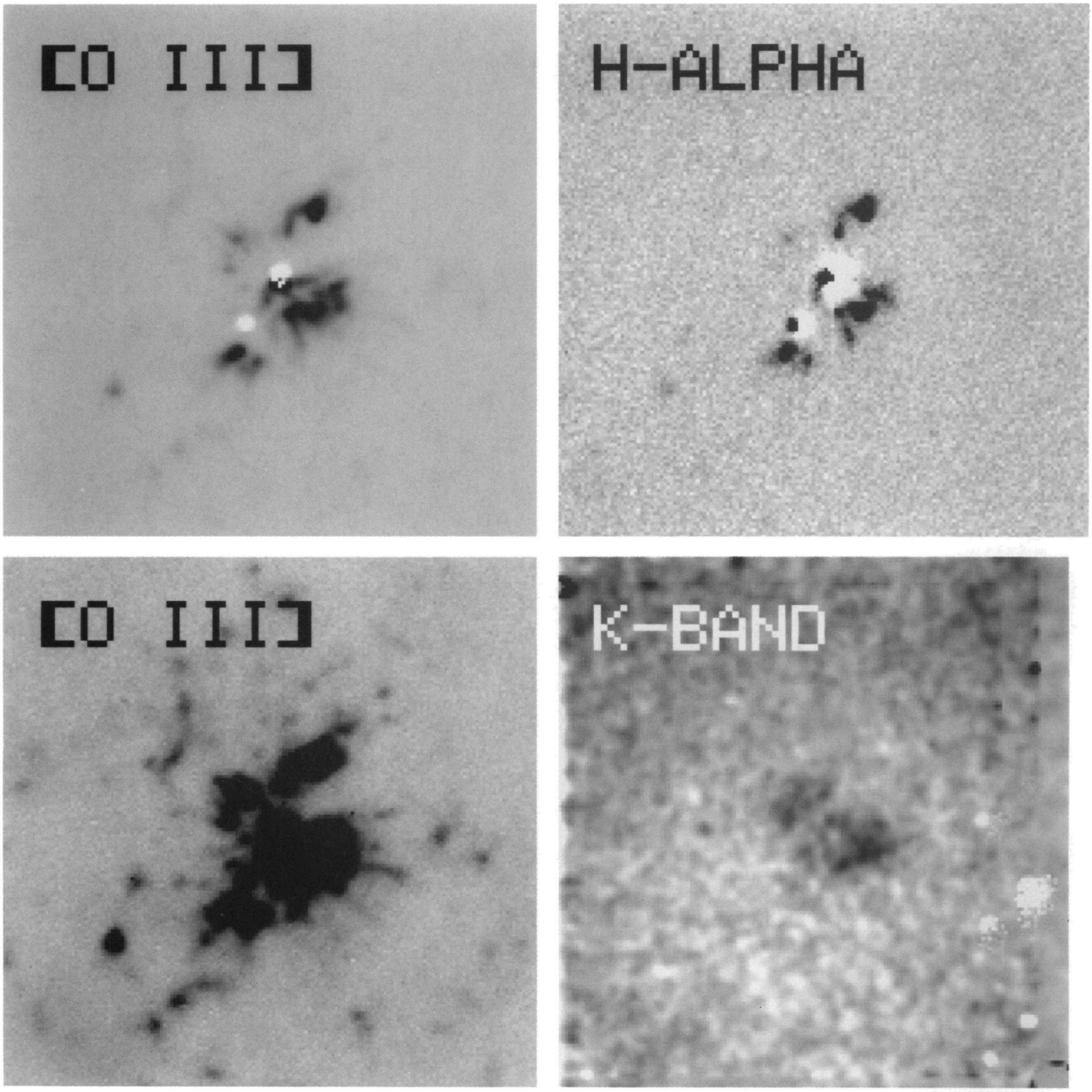

FIG. 2.—Montage of aligned and scaled images of the inner region of A30. The two panels on the left show the [O III] data stretched by different amounts to show more details of the inner structure. The upper right-hand panel shows the Hα image, although the emission seen is mainly from [N II] (see text). The lower right-hand panel shows the background- and central-star–subtracted *K*-band image to the same scale. Each panel is 49″ on a side, with north at the top and east to the left. The optical 6100 Å continuum image has been subtracted from the upper two panels, leaving stellar residuals at the positions of the central star and another star to the southeast.

(BORKOWSKI et al. (see 435, 723)